


Electrical insulation properties of the perfluoroketone C₅F₁₀O

Journal Article**Author(s):**

Chachereau, Alise ; Hösl, Andreas ; Franck, Christian 

Publication date:

2018

Permanent link:

<https://doi.org/10.3929/ethz-b-000262555>

Rights / license:

[Creative Commons Attribution-NonCommercial-NoDerivs 3.0 Unported](#)

Originally published in:

Journal of Physics D: Applied Physics 51(33), <https://doi.org/10.1088/1361-6463/aad174>

ACCEPTED MANUSCRIPT

Electrical insulation properties of the perfluoroketone C5F10O

To cite this article before publication: Alise Chachereau *et al* 2018 *J. Phys. D: Appl. Phys.* in press <https://doi.org/10.1088/1361-6463/aad174>

Manuscript version: Accepted Manuscript

Accepted Manuscript is “the version of the article accepted for publication including all changes made as a result of the peer review process, and which may also include the addition to the article by IOP Publishing of a header, an article ID, a cover sheet and/or an ‘Accepted Manuscript’ watermark, but excluding any other editing, typesetting or other changes made by IOP Publishing and/or its licensors”

This Accepted Manuscript is © 2018 IOP Publishing Ltd.

During the embargo period (the 12 month period from the publication of the Version of Record of this article), the Accepted Manuscript is fully protected by copyright and cannot be reused or reposted elsewhere. As the Version of Record of this article is going to be / has been published on a subscription basis, this Accepted Manuscript is available for reuse under a CC BY-NC-ND 3.0 licence after the 12 month embargo period.

After the embargo period, everyone is permitted to use copy and redistribute this article for non-commercial purposes only, provided that they adhere to all the terms of the licence <https://creativecommons.org/licenses/by-nc-nd/3.0>

Although reasonable endeavours have been taken to obtain all necessary permissions from third parties to include their copyrighted content within this article, their full citation and copyright line may not be present in this Accepted Manuscript version. Before using any content from this article, please refer to the Version of Record on IOPscience once published for full citation and copyright details, as permissions will likely be required. All third party content is fully copyright protected, unless specifically stated otherwise in the figure caption in the Version of Record.

View the [article online](#) for updates and enhancements.

Electrical insulation properties of the perfluoroketone $C_5F_{10}O$

A. Chachereau¹, A. Hösl¹, C. M. Franck¹

¹Power Systems and High Voltage Laboratories, ETH Zurich, Physikstr. 3, 8092 Zurich, Switzerland

E-mail: alisec@ethz.ch

Abstract. The electrical insulation properties of pure $C_5F_{10}O$ and of $C_5F_{10}O/N_2$ and $C_5F_{10}O/CO_2$ mixtures are investigated in a pulsed Townsend setup. The electron rate and transport coefficients and the density-reduced critical electric field of these mixtures are obtained, and a synergy effect is observed in $C_5F_{10}O/N_2$ and $C_5F_{10}O/CO_2$ mixtures. The total electron attachment cross section of $C_5F_{10}O$ is estimated based on the attachment rate to $C_5F_{10}O$ in diluted $C_5F_{10}O/N_2$ and $C_5F_{10}O/CO_2$ mixtures.

Introduction

The perfluoroketone $CF_3C(=O)CF(CF_3)_2$, which we refer to in the following as $C_5F_{10}O$, has been recently proposed as an environment-friendly alternative to SF_6 in high voltage gaseous electrical insulation [1, 2]. The manufacturer reports a low toxicity and recommends an occupational exposure limit of 225 ppm for $C_5F_{10}O$ [3]. SF_6 has excellent electric insulation properties, yet its global warming potential (GWP) on a hundred year time horizon is 23 500 relative to CO_2 [4]. By contrast, the GWP of $C_5F_{10}O$ is smaller than 1 [3] due to the rapid photolysis of $C_5F_{10}O$ in the atmosphere, similar to the perfluoroketone $C_2F_5C(O)CF(CF_3)_2$ [5]. $C_5F_{10}O$ has a boiling point of 26.9 °C [6], therefore, it does not have a sufficiently high vapor pressure to be used as a single gas in high voltage insulation, but has to be admixed with a carrier gas of high vapor pressure. A pilot gas insulated substation with $C_5F_{10}O$ is in operation in Zurich, Switzerland, using a mixture of 5.6% $C_5F_{10}O$, 11.1% O_2 and 83.3% CO_2 in the high voltage switchgear with a rated voltage of 170 kV, and $C_5F_{10}O$ /synthetic air mixtures in the medium voltage panels [7, 8]. Medium voltage ring main units using $C_5F_{10}O$ /synthetic air mixtures are also available [9]. Several investigations have reported breakdown voltages of $C_5F_{10}O$ mixtures with synthetic air, CO_2 , and $CO_2 + O_2$ [2, 10, 11], and the effective ionization coefficient of $C_5F_{10}O$ mixtures with synthetic air has also been recently measured by Aints et al. in a steady-state Townsend experiment [12].

In the present work, we consider mixtures of $C_5F_{10}O$ with the carrier gases N_2 and CO_2 . We present measurement results in diluted mixtures of $C_5F_{10}O$ in N_2 and in CO_2 , and use these to estimate the electron attachment cross section of $C_5F_{10}O$. We report the rate coefficients of ionization, attachment, and effective ionization, as well as the electron drift velocity and the longitudinal electron diffusion coefficient in pure $C_5F_{10}O$. Furthermore, we measure the properties of

$C_5F_{10}O/CO_2$ and $C_5F_{10}O/N_2$ mixtures with $C_5F_{10}O$ percentages up to 40%, in order to investigate the synergism of the density-reduced critical electric field. We compare our results with those of Aints et al. We make all our data available on the database ETHZ [13] from the LXcat project.

1. Methods

1.1. Swarm experiment

1.1.1. Experimental setup Most of the measurements were performed in the pulsed Townsend setup that was described in [14]. The latest measurements in pure $C_5F_{10}O$ were performed in a newer setup [15]. A principle schematic valid for both setups is shown in figure 1. Each setup comprises a stainless steel vessel containing two Rogowski electrodes. A voltage is applied across the electrodes, resulting in a homogeneous electric field in the electrode gap. The gases under study are filled in the vessel as described in section 1.1.2. The cathode is made of two parts, a bulk cathode with a hole in its center, in which a photocathode is inserted. The photocathodes used for the present measurements were quartz slabs coated with a 15 nm magnesium layer, which is again overcoated with a 5 nm palladium layer. A pulsed UV-laser with a wavelength of 266 nm and a pulse duration of 1.5 ns FWHM illuminates the photocathode from the back. Photoelectrons are released from the photocathode into the gap between the electrodes and initiate an electron avalanche. The electrons produce positive ions by impact ionization, and negative ions by electron attachment. The displacement current resulting from the drift of the electrons and ions in the electric field is measured. The resistance R_1 and capacitance C in figure 1 are needed to ensure that the recharging current of the electrode capacitance, which compensates the electron emission from the cathode, is spread over a long time period (a few millisecond),

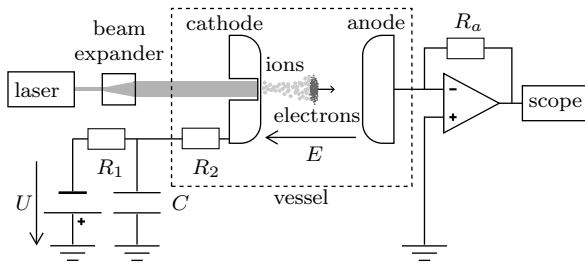


Figure 1. Schematic of the pulsed Townsend experiment ($R_1 \sim 1 \text{ M}\Omega$, $R_2 \sim 100 \Omega$, $C \sim 1 \text{ nF}$).

so that it is negligible compared to the displacement current of electrons and ions.

1.1.2. Gas purity The vessel has a base pressure of $1 \times 10^{-6} \text{ Pa}$. In order to fill a gas or gas mixture, the content of the inlet pipes is first evacuated through the vessel. Then, each of the inlet pipes is flushed with one of the gases under study. Finally, the vessel is evacuated again and closed. The residual pressure in the vessel before the gas is filled is below 0.1 Pa . The gases are then filled one after the other, starting with the least abundant gas in the gas mixture. The gases used in the present work are $\text{C}_5\text{F}_{10}\text{O}$ with a purity of at least 99.5 mole % (3M), N_2 with a purity of 6.0 (Carbagas), and CO_2 with a purity of 4.8 (Carbagas).

1.2. Measurement analysis

The measured current is the sum of the electron and ion currents. These two components are separated using an iterative procedure [16] and analyzed as follows.

1.2.1. Electron current analysis The electron current analysis was described in detail in a previous publication [16]; the physical model is briefly described here to introduce the relevant quantities. Assuming that the one-dimensional electron density along the avalanche propagation axis is Gaussian, the electron current I_e is expressed analytically for $t \geq 0$ as [14, 16]

$$I_e(t) = \frac{I_0}{2} e^{k_{\text{eff}} N t} \left(1 - \text{erf} \left(\frac{t - T_e}{\sqrt{2\tau_D t}} \right) \right), \quad (1)$$

$$I_0 = \frac{N_e(0)q_0}{T_e}, \quad (2)$$

where I_0 is the electron current at time $t = 0$, k_{eff} is the effective ionization rate coefficient, N is the number density of the gas, T_e is the electron drift time, which relates to the bulk electron drift velocity w_e via $T_e = d/w_e$, τ_D is the characteristic time for longitudinal electron diffusion, which relates to the longitudinal diffusion coefficient D_L via $2D_L = w_e^2 \tau_D$, $N_e(0)$ is the initial number of electrons and q_0 is the elementary charge.

1.2.2. Ion current analysis A simple model for the ion current I_{ion} was described previously [16] for the case where only one type of cation and one type of anion are present. This approach fails for instance when two types of negative ions (or two types of positive ions) with different drift velocities are present. This can occur due to the existence of several attachment (or several ionization) processes, or due to ion conversion or charge transfer. With a more sophisticated approach, it is possible to analyze cases with several anion species, including even ion kinetics [17], but this requires an extensive knowledge of the kinetic processes, which is not available in the case of $\text{C}_5\text{F}_{10}\text{O}$.

We introduce here a simpler analysis which allows us to obtain only the ionization and attachment rate coefficients k_i and k_a , but makes no assumptions on the number of ion species nor on the number of ionization, attachment and ion conversion processes. We still assume that the effective ionization rate coefficient k_{eff} is simply given by the difference between the ionization and attachment rate coefficients

$$k_{\text{eff}} = k_i - k_a, \quad (3)$$

explicitly excluding electron detachment and any other process that could lead to secondary electron production. This analysis relies furthermore on the fact that k_{eff} and $N_e(0)$ are already known from the electron current analysis. For simplicity, we neglect electron diffusion in the following calculations so that the number of electrons at an instant $0 \leq t \leq T_e$ is given by

$$N_e(t) = N_e(0) \exp(k_{\text{eff}} N t). \quad (4)$$

The time integral of the measured current I_{exp} gives the total amount of charge that transits through the gap between the electrodes. Dividing it by the elementary charge q_0 , we obtain the number $N_{\text{charges}}^{\text{final}}$ of charge carriers which virtually cross the gap between the electrodes

$$N_{\text{charges}}^{\text{final}} = \frac{1}{q_0} \int_0^\infty I_{\text{exp}}(t) dt. \quad (5)$$

The initial number of charge carriers is given by the initial number of photoelectrons $N_e(0)$ released at the cathode. Each of the initial elementary charges $N_e(0)$ effectively crosses the gap between the electrodes (either as an electron or as an anion if the electron is attached as shown in figure 2) and therefore contributes to $N_{\text{charges}}^{\text{final}}$. Along the way, electrons may ionize a particle, creating a positive ion and a new free electron. For each ionization event, an additional elementary charge will cross completely the gap between electrodes as illustrated in figure 2: the newly freed electron covers the remaining distance towards the anode, whereas the newly created cation covers the distance back to the cathode. As a result, $N_{\text{charges}}^{\text{final}}$ is the sum of

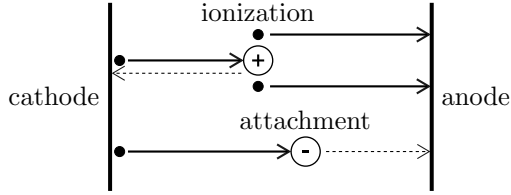


Figure 2. Schematic of the transit of charge carriers (• electron, ⊕ cation, ⊖ anion) between the electrodes.

the initial number of photoelectrons and the number of ionization events, i.e. the number of positive ions $N_p(T_e)$:

$$N_{\text{charges}}^{\text{final}} = N_e(0) + N_p(T_e). \quad (6)$$

The number of ionization events during a small time interval $[t, (t + dt)]$ is related to the ionization rate coefficient k_i and the number of electrons present at time t as

$$dN_p(t) = k_i N N_e(t) dt \quad (7)$$

The final number of ionization events is reached once the electrons have been absorbed by the anode, i.e. at time T_e . It is obtained by integrating the cation production between instants 0 and T_e

$$\begin{aligned} N_p(T_e) &= k_i N \int_0^{T_e} N_e(t) dt \\ &= N_e(0) \frac{k_i}{k_{\text{eff}}} (\exp(k_{\text{eff}} N T_e) - 1) \\ &= \frac{k_i}{k_{\text{eff}}} (N_e(T_e) - N_e(0)). \end{aligned} \quad (8)$$

Replacing equation (8) into (6) yields

$$N_{\text{charges}}^{\text{final}} = N_e(0) + \frac{k_i}{k_{\text{eff}}} (N_e(T_e) - N_e(0)). \quad (9)$$

And this yields for k_i and k_a

$$k_i = k_{\text{eff}} \frac{N_{\text{charges}}^{\text{final}} - N_e(0)}{N_e(T_e) - N_e(0)}, \quad (10)$$

$$k_a = k_i - k_{\text{eff}} = k_{\text{eff}} \frac{N_{\text{charges}}^{\text{final}} - N_e(T_e)}{N_e(T_e) - N_e(0)}. \quad (11)$$

The key assumption of this method is the absence of ionization events after the electron drift time T_e . The occurrence of ionization events after T_e is not accounted for in the calculation of $N_p(T_e)$ with equation (8), using the present method would thus result in overestimating k_i and k_a .

1.2.3. Density-reduced critical electric field

The density-reduced critical electric field $(E/N)_{\text{crit}}$ of a gas is defined as the E/N ratio for which $k_{\text{eff}} = 0$, that is $k_i = k_a$. For $E/N < (E/N)_{\text{crit}}$, electron attachment is dominating over ionization. For $E/N > (E/N)_{\text{crit}}$, ionization dominates over

electron attachment. Therefore, $(E/N)_{\text{crit}}$ is a figure of merit for electrical insulation, it is the minimum E/N ratio for which an electrical discharge can be self-sustained. The $(E/N)_{\text{crit}}$ of a gas mixture cannot be predicted based solely on the $(E/N)_{\text{crit}}$ of the individual components since it depends largely on the electron energy distribution in the gas mixture. A gas mixture is said to have a synergy when its $(E/N)_{\text{crit}}$ is larger than the sum of the $(E/N)_{\text{crit}}$ of its components weighted by their mole fractions in the mixture [18]. In the present work, the $(E/N)_{\text{crit}}$ of different $C_5F_{10}O/N_2$ and $C_5F_{10}O/CO_2$ mixtures is obtained as the zero-crossing of the measured k_{eff} versus E/N curves.

1.2.4. Estimating the total electron attachment cross section The total attachment cross section of $C_5F_{10}O$ is estimated using two methods, a linear inversion method and a Gaussian expansion method, which were described previously [19]. These methods require as input the effective ionization coefficient measured in diluted mixtures of $C_5F_{10}O$ with different carrier gases, in the present case N_2 and CO_2 , and the knowledge of the electron energy distribution function (EEDF) in the carrier gases. In the present work the EEDF in N_2 and CO_2 is obtained by solving the Boltzmann equation in the two-term approximation using the solver Bolsig+ [20], with Biagi's cross section set for N_2 [21] and Phelps' cross section set for CO_2 [22]. The effective ionization rate coefficient, electron drift velocity and diffusion coefficients calculated in pure N_2 and in pure CO_2 are shown in figures 5 and 4 respectively. Both methods rely on the assumption that the $C_5F_{10}O$ admixture does not disturb the electron energy distribution function of the carrier gas. The linear inversion method has the advantage of making no assumption on the shape of the cross section and requiring no initial guess of the solution. We denote $\sigma_a^{(\text{li})}$ the cross section obtained by this method. The Gaussian expansion is an optimization method where the shape of the cross section is approximated by the sum of several Gaussian functions. We denote $\sigma_a^{(\text{ge})}$ the cross section obtained by this method. In the present case, the cross section is well fitted with three terms, i.e.

$$\sigma_a^{(\text{ge})}(\varepsilon) = \sum_{i=1}^3 c_i e^{-(\varepsilon - \varepsilon_i)^2 / (2s_i^2)}, \quad (12)$$

where c_i , ε_i and s_i are the amplitude, position and width of the Gaussian peaks, determined by the fit.

2. Results

2.1. Diluted $C_5F_{10}O/N_2$ and $C_5F_{10}O/CO_2$ mixtures

This section presents the electron swarm parameters obtained in $C_5F_{10}O/N_2$ and $C_5F_{10}O/CO_2$ mixtures

Table 1. Overview of the measurements in the diluted C₅F₁₀O/N₂ and C₅F₁₀O/CO₂ mixtures.

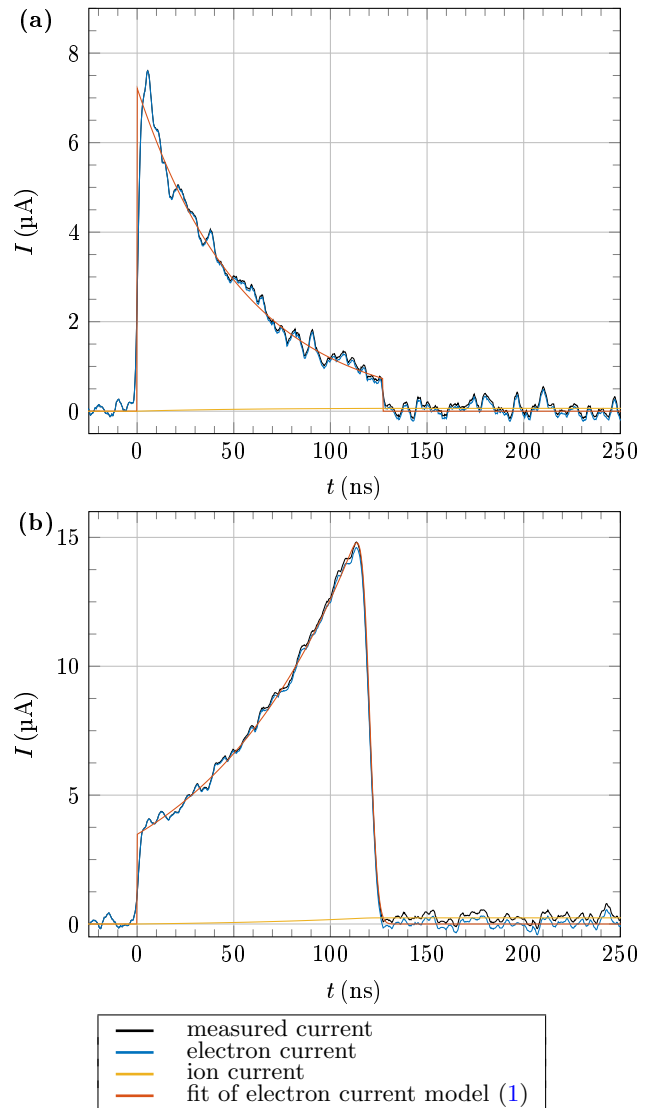
buffer gas	C ₅ F ₁₀ O (mol%)	(<i>E/N</i>)-range (Td)	pressures (kPa)
N ₂	0	5 - 180	2, 10
	0.13	5 - 140	2, 10
	0.25	50 - 140	2, 10
CO ₂	0	5 - 140	2, 10
	0.26	5 - 110	2, 10
	0.50	6 - 26	10
	1.00	108 - 130	2, 10

where the percentage of C₅F₁₀O is smaller than 1%. While these mixtures are not directly of interest for electrical insulation, they allow us to probe the attachment cross section of C₅F₁₀O, using the methods described in section 1.2.4. An overview of the investigated mixtures is given in table 1. Example measurements in the mixture of 1% C₅F₁₀O in CO₂ are shown in figure 3 for two different ratios of the electric field over gas density *E/N*. The electron current is fitted satisfyingly by the analytic model (1). It results from the analytical model (1) that the exponential decrease of the electron current in figure 3(a) is due to a negative value of *k*_{eff}, in other terms, the electron attachment rate is larger than the ionization rate *k*_a > *k*_i, i.e. *E/N* < (*E/N*)_{crit}. In figure 3(b), the electron current is exponentially increasing with time, which corresponds to *k*_a < *k*_i, i.e. *E/N* > (*E/N*)_{crit}.

The obtained effective ionization rate coefficient, electron drift velocity and diffusion coefficient are shown in figures 5 for N₂ mixtures and figure 4 for CO₂ mixtures. The electron drift velocity and diffusion coefficient are not affected by the addition of a small amount of C₅F₁₀O in N₂ and CO₂, whereas the effective ionization coefficient in diluted C₅F₁₀O mixtures is decreasing with increasing C₅F₁₀O content due to electron attachment to C₅F₁₀O.

2.2. Electron attachment cross section

Figure 6 shows the estimations of the attachment cross sections $\sigma_a^{(li)}$ and $\sigma_a^{(ge)}$ of C₅F₁₀O obtained with the linear inversion method and the Gaussian expansion method, respectively. The electron attachment cross section of SF₆ is shown for comparison, it is taken from the Biagi database [21], which used the results from Braun et al [23] and Christophorou and Olthoff [24]. A good agreement is obtained between both estimations $\sigma_a^{(li)}$ and $\sigma_a^{(ge)}$, which is encouraging as to the uniqueness of the solution. To verify the accuracy of those estimations, the values of *k*_{eff} in C₅F₁₀O mixtures are calculated from the cross sections $\sigma_a^{(li)}$

**Figure 3.** Current versus time in the mixture of 1% C₅F₁₀O in CO₂, at a pressure of 10 kPa, for an electrode spacing of 19 mm, and for a reduced electric field *E/N* of (a) 110 Td and (b) 124 Td.

and $\sigma_a^{(ge)}$ as

$$k_{\text{eff}}^{[\text{C}_5\text{F}_{10}\text{O mixture}]} = (1-x)k_{\text{eff}}^{[\text{carrier gas}]} - x\sqrt{\frac{2}{m_e}} \int_0^\infty \sigma_a \varepsilon f^{[\text{carrier gas}]} d\varepsilon, \quad (13)$$

where *x* is the mole fraction of C₅F₁₀O in the mixture, *m*_e is the electron mass, *k*_{eff}^[carrier gas] is the effective ionization rate coefficient in the carrier gas and *f*^[carrier gas] is the electron energy distribution function in the carrier gas. Both *k*_{eff}^[carrier gas] and *f*^[carrier gas] are calculated with Bolsig+ as indicated in section 1.2.4. The calculations of *k*_{eff} using $\sigma_a^{(li)}$ and $\sigma_a^{(ge)}$ are shown in figures 5(a) and 4(a) using dashed and dotted lines. The calculations agree perfectly with each other and with the measured values of *k*_{eff}. Thus, $\sigma_a^{(li)}$ and $\sigma_a^{(ge)}$

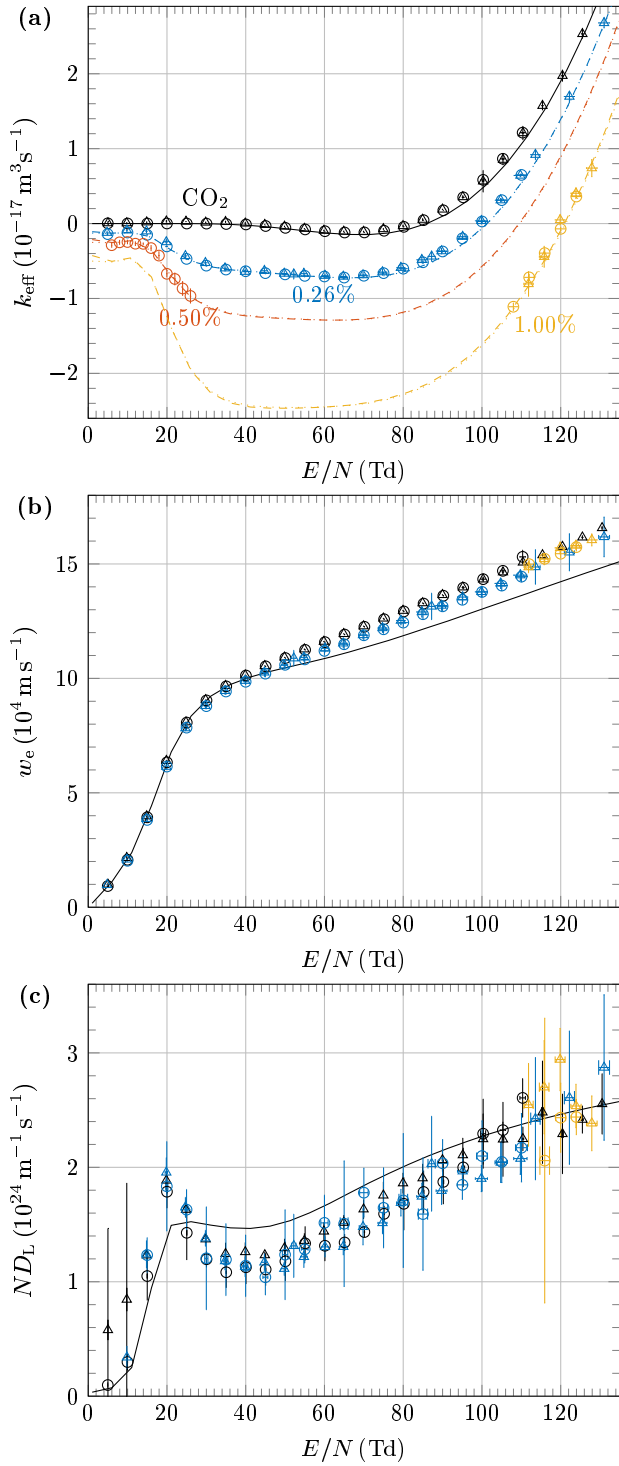


Figure 4. (a) Effective ionization rate coefficient, (b) drift velocity and (c) diffusion coefficient as functions of E/N in $C_5F_{10}O/CO_2$ mixtures. The gas mixtures are color-coded, the $C_5F_{10}O$ percentages being indicated in figure (a). The gas pressures are indicated with different marker shapes (Δ 2 kPa, \circ 10 kPa). The full lines in (a), (b) and (c) correspond to k_{eff} , w_e and ND_L in CO_2 , calculated using Bolsig+. The dashed and dotted lines in (a) correspond to calculations of k_{eff} in the $C_5F_{10}O/CO_2$ mixtures obtained with equation (13) using $\sigma_a^{(ii)}$ and $\sigma_a^{(ge)}$, respectively.

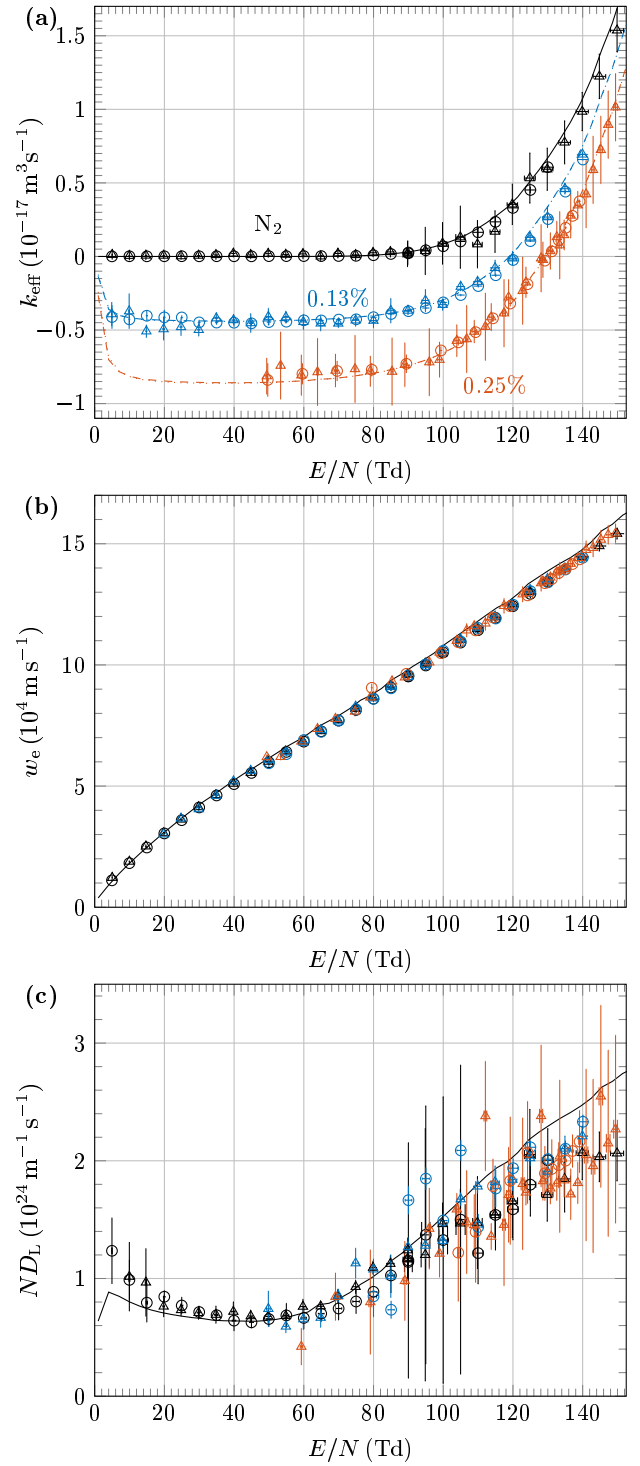


Figure 5. (a) Effective ionization rate coefficient, (b) electron drift velocity and (c) electron diffusion coefficient as functions of E/N in $C_5F_{10}O/N_2$ mixtures. The gas mixtures are color-coded, the $C_5F_{10}O$ percentages being indicated in figure (a). The gas pressures are indicated with different marker shapes (Δ 2 kPa, \circ 10 kPa). The full lines in (a), (b) and (c) correspond to k_{eff} , w_e and ND_L in N_2 , calculated using Bolsig+. The dashed and dotted lines in (a) correspond to calculations of k_{eff} in the $C_5F_{10}O/N_2$ mixtures obtained with equation (13) using $\sigma_a^{(ii)}$ and $\sigma_a^{(ge)}$, respectively.

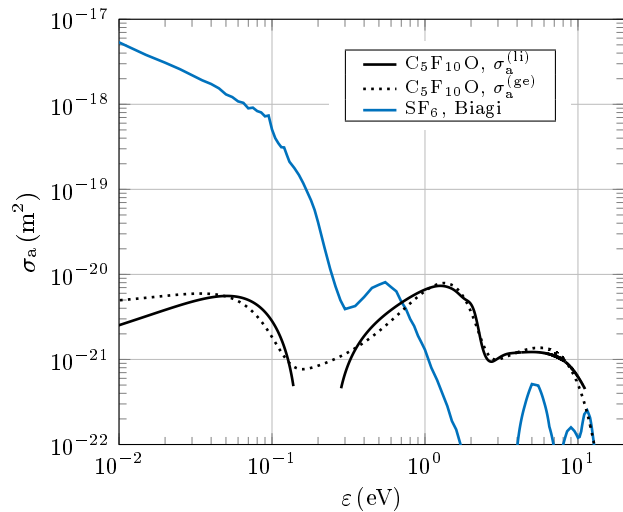


Figure 6. Total attachment cross section of SF_6 and estimated total electron attachment cross section of $\text{C}_5\text{F}_{10}\text{O}$.

are equally good estimations of the attachment cross section of $\text{C}_5\text{F}_{10}\text{O}$. The slight difference between $\sigma_a^{(\text{li})}$ and $\sigma_a^{(\text{ge})}$ at low electron energies $\varepsilon \lesssim 0.05$ eV, results in a small divergence in the calculated k_{eff} , visible only for $E/N < 6$ Td in the diluted CO_2 mixtures of figure 4(a). Since this low E/N range was not covered in the present measurements, the attachment cross section cannot be precisely resolved at electron energies below 0.05 eV, but is in the right order of magnitude. The estimated attachment cross section of $\text{C}_5\text{F}_{10}\text{O}$, $\sigma_a^{(\text{li})}$ and $\sigma_a^{(\text{ge})}$, feature three attachment peaks. A very narrow peak is found at 0.05 eV, although the actual peak position might be at lower energies since this range is not well resolved. The main attachment peak is at 1.3 eV and a third peak is found at about 5.5 eV. Since the present measurements are not extremely sensitive on the exact shape of the cross section for energies higher than 2 eV, the peak observed at about 5.5 eV could be in fact the superposition of several peaks in the range 2–10 eV. The attachment cross section of SF_6 is also shown in figure 6 for comparison. $\text{C}_5\text{F}_{10}\text{O}$ has a much lower attachment cross section than SF_6 at low energies, but a much larger attachment cross sections at energies above 0.7 eV and up to 10 eV.

2.3. Results in pure $\text{C}_5\text{F}_{10}\text{O}$

Measurements were performed in pure $\text{C}_5\text{F}_{10}\text{O}$ over a large pressure range, from 100 Pa to 2 kPa. At low pressures, a large range of E/N is covered, from 50 Td to 900 Td, whereas at high pressures the range is restricted to a narrow E/N band around the critical field $(E/N)_{\text{crit}}$. Example measurements carried out in pure $\text{C}_5\text{F}_{10}\text{O}$ at the pressure 100 Pa are shown in figures 7 and 8. Figure 9 shows the ionization,

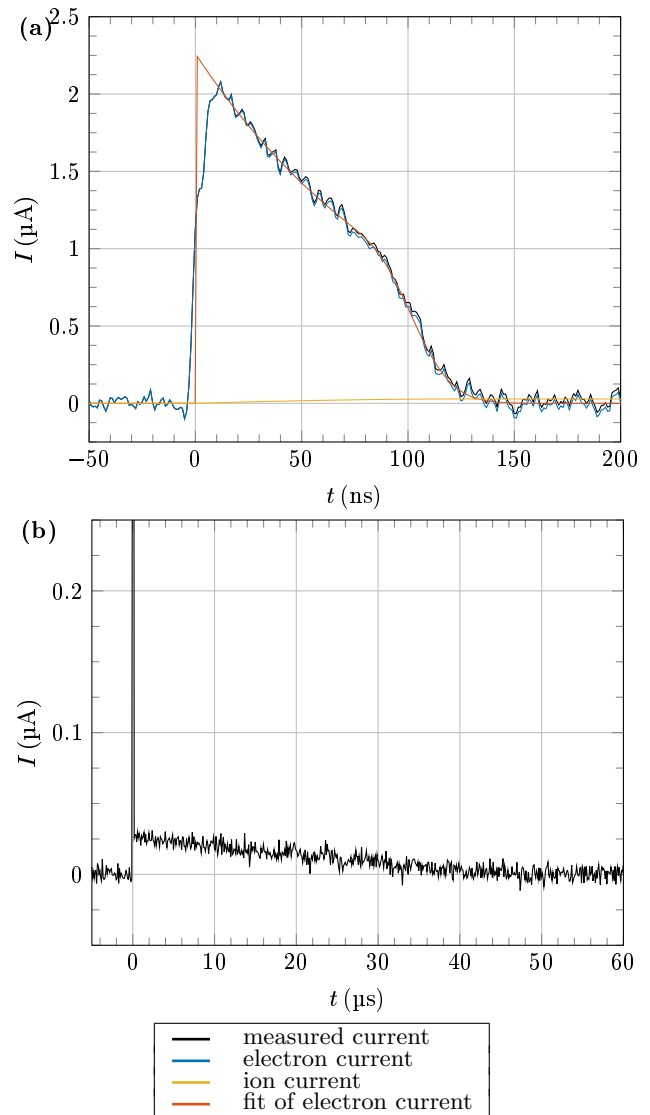


Figure 7. Current versus time in pure $\text{C}_5\text{F}_{10}\text{O}$, at a pressure of 0.1 kPa, for an electrode spacing of 25 mm, and for a reduced electric field E/N of 698 Td (a) on the electronic timescale and (b) on the ionic timescale.

attachment and effective ionization rate coefficients, as well as the electron drift velocity and diffusion coefficient obtained in pure $\text{C}_5\text{F}_{10}\text{O}$. The results are independent of the gas pressure. In particular, the fact that the obtained values of k_i and k_a are independent of the gas pressure implies that no electron detachment occurs in $\text{C}_5\text{F}_{10}\text{O}$, as equations (10) and (11) would fail if it were the case. A certain spread is observed in the values of the effective ionization rate coefficient of $\text{C}_5\text{F}_{10}\text{O}$ around the critical electric field. The density-reduced critical electric field of $\text{C}_5\text{F}_{10}\text{O}$ is 757 ± 10 Td.

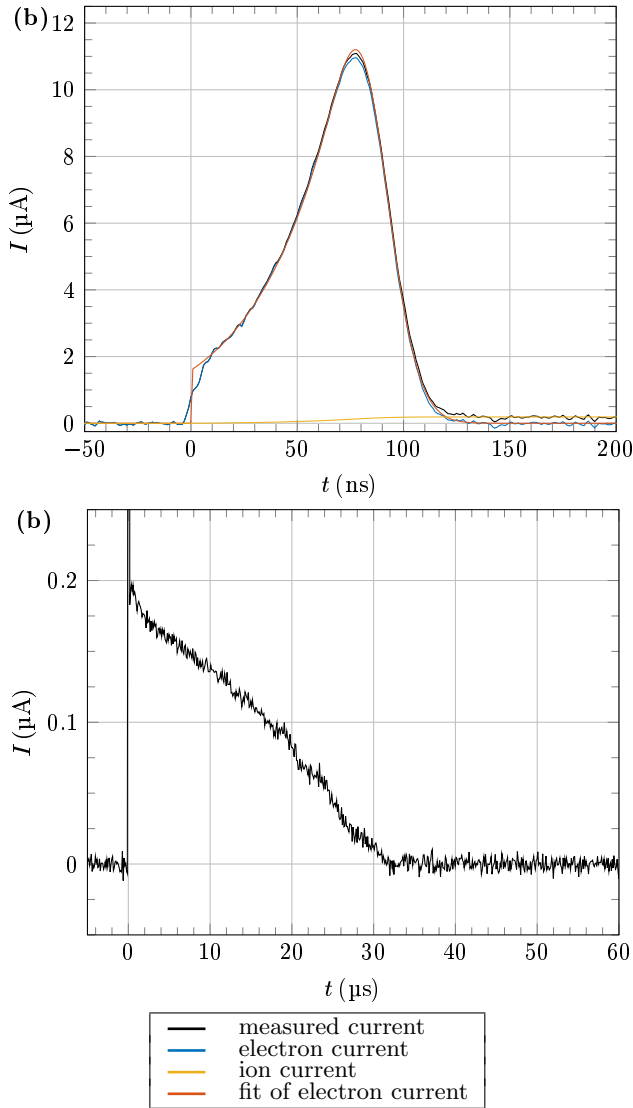


Figure 8. Current versus time in pure $C_5F_{10}O$, at a pressure of 0.1 kPa, for an electrode spacing of 25 mm, and for a reduced electric field E/N of 898 Td (a) on the electronic timescale and (b) on the ionic timescale.

2.4. Synergism in $C_5F_{10}O/N_2$ and $C_5F_{10}O/CO_2$ mixtures

In order to study the synergism in the density-reduced critical electric field, we measure different $C_5F_{10}O/N_2$ and $C_5F_{10}O/CO_2$ mixtures with up to 40% $C_5F_{10}O$. An overview of the measurements is given in table 2. Example measurements in the mixture of 12% $C_5F_{10}O$ in N_2 at 10 kPa are shown in figure 10. For these measurements, the analytic fit of the signal was rather insensitive on the diffusion coefficient, which could take any value between 1×10^{24} to $2 \times 10^{25} \text{ m}^{-1} \text{ s}^{-1}$, therefore, we do not report the electron diffusion coefficient. Measurements at lower pressures would have been preferable to obtain the diffusion coefficient, but would have yielded less accurate values for

Table 2. Overview of the measurements in the $C_5F_{10}O/N_2$ and $C_5F_{10}O/CO_2$ mixtures.

buffer gas	$C_5F_{10}O$ mol%	(E/N) -range (Td)	pressures (kPa)
N_2	0	5 - 180	2, 10
	1.01	110 - 186	2, 10
	4.04	198 - 212	2, 4, 10
	8.06	238 - 250	10
	12.03	268 - 276	10
	19.96	324 - 332	10
	30.06	384 - 390	10
39.85	440 - 445	10	
CO_2	0	5 - 140	2, 10
	1.00	108 - 130	2, 10
	4.09	157 - 167	10
	8.13	195 - 207	10
	12.01	225 - 235	10
	20.03	288 - 295	10
	30.03	354 - 361	10
39.87	415 - 422	10	

the effective ionization rate coefficient, which was prioritized here. Figures 12 and 11 show the effective ionization rate coefficient, the electron drift velocity and the longitudinal electron diffusion coefficient obtained in $C_5F_{10}O/N_2$ and $C_5F_{10}O/CO_2$ mixtures respectively. A large increase of the density-reduced critical electric field $(E/N)_{crit}$ is observed with increasing $C_5F_{10}O$ content. The obtained $(E/N)_{crit}$ values in $C_5F_{10}O/N_2$ and $C_5F_{10}O/CO_2$ mixtures are summarized in figure 13 and compared to the $(E/N)_{crit}$ of $C_5F_{10}O$ /synthetic air mixtures from Aints et al. [12] and that of SF_6/N_2 and SF_6/CO_2 mixtures [25]. We observe a synergy effect in both the $C_5F_{10}O/N_2$ and the $C_5F_{10}O/CO_2$ mixtures, but it is more pronounced in the $C_5F_{10}O/N_2$ mixtures. Mixtures of $\sim 26\%$ $C_5F_{10}O$ in N_2 and of $\sim 30\%$ $C_5F_{10}O$ in CO_2 have the same density-reduced critical electric field as pure SF_6 . The value of 770 ± 25 Td for the $(E/N)_{crit}$ of pure $C_5F_{10}O$ obtained by Aints et al. is in good agreement with the range of 757 ± 10 Td obtained in the present study. And the $(E/N)_{crit}$ values obtained by Aints et al. for $C_5F_{10}O$ /synthetic air mixtures are quite similar to the present values obtained in $C_5F_{10}O/N_2$ mixtures.

3. Discussion

3.1. Electron attachment to $C_5F_{10}O$

Electron attachment to fluorinated ketones has not been extensively studied. To our knowledge, only Illenberger and Meinke [26] reported measurements of electron attachment to perfluoroacetone using a crossed beam experiment and mass spectrometric detection of the anions. They observed strong parent ion formation peaking towards 0 eV as well as multiple

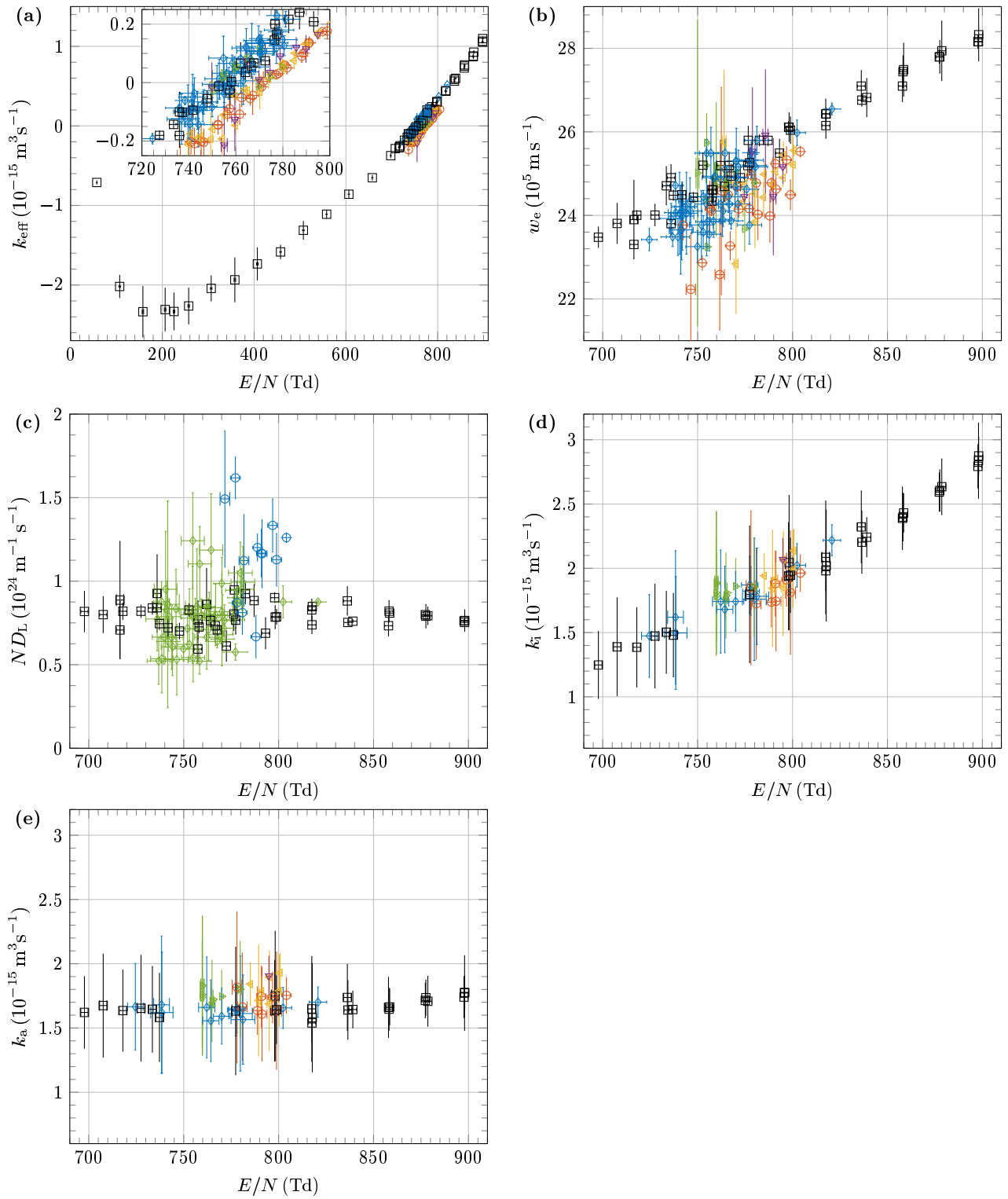


Figure 9. (a) Effective ionization rate coefficient, (b) electron drift velocity, (c) electron diffusion coefficient, (d) ionization rate coefficient and (e) attachment rate coefficient as functions of E/N in $C_5F_{10}O$, at different gas pressures (\square 0.1 kPa, \diamond 0.2 kPa, \circ 0.5 kPa, \triangleleft 1 kPa, ∇ 1.5 kPa, \triangleright 2 kPa).

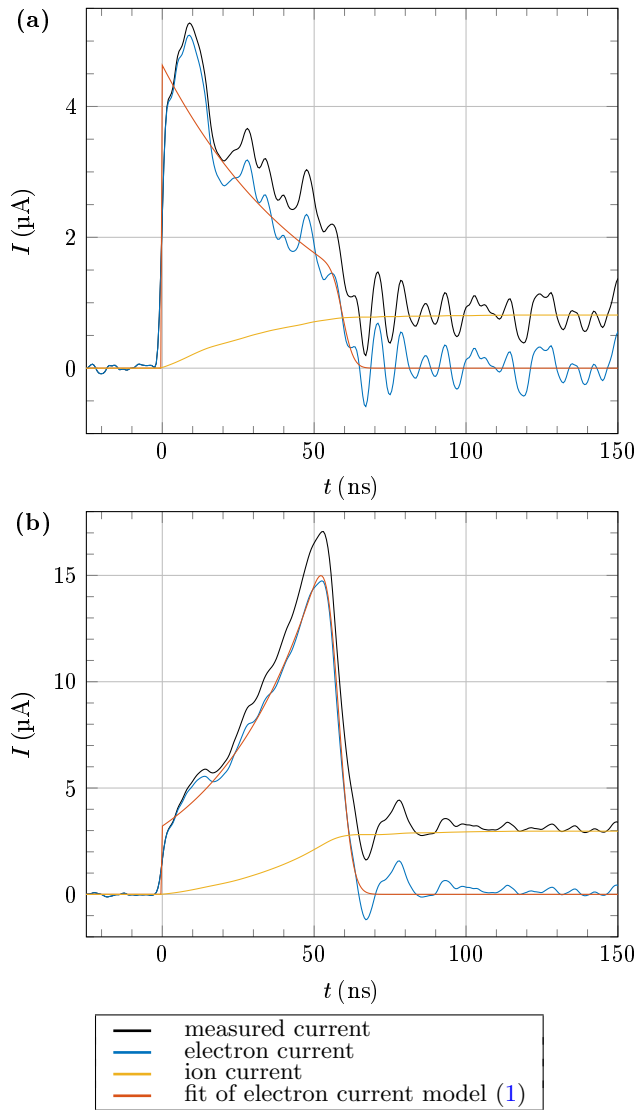


Figure 10. Current versus time in the mixture of 12% $\text{C}_5\text{F}_{10}\text{O}$ in N_2 , at a pressure of 10 kPa, for an electrode spacing of 13 mm, and for a reduced electric field E/N of (a) 268 Td and (b) 276 Td.

dissociative attachment peaks in the range of 2–12 eV. We observe a somewhat different picture for the perfluoroketone $\text{C}_5\text{F}_{10}\text{O}$. The effective ionization rate coefficient in $\text{C}_5\text{F}_{10}\text{O}/\text{N}_2$ and $\text{C}_5\text{F}_{10}\text{O}/\text{CO}_2$ mixtures shown in figures 5(a) and 4(a) is lowest at intermediate E/N ratios, from about 30 Td to 80 Td, which suggests that electron attachment to $\text{C}_5\text{F}_{10}\text{O}$ occurs mainly at electron energies above thermal. Accordingly, the estimated electron attachment cross section features only a small attachment peak at low energies possibly being parent ion attachment, and a main attachment peak at 1.3 eV. We do observe substantial attachment in the range 3–11 eV which could be the superposition of multiple dissociative attachment peaks, similarly to perfluoroacetone.

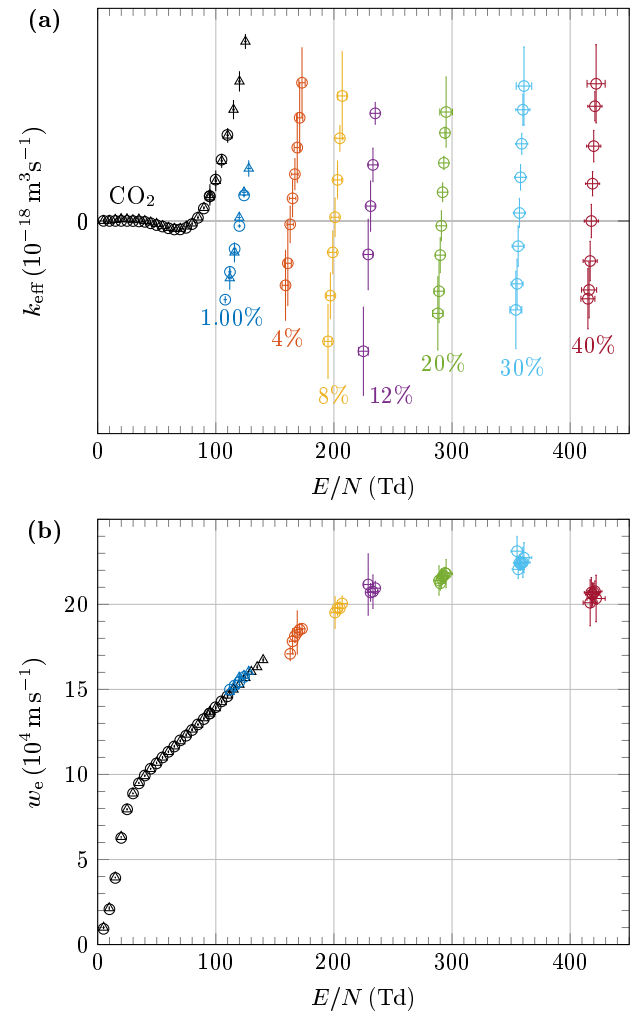


Figure 11. (a) Effective ionization rate coefficient and (b) electron drift velocity as functions of E/N in $\text{C}_5\text{F}_{10}\text{O}/\text{CO}_2$ mixtures. The gas mixtures are color-coded, the $\text{C}_5\text{F}_{10}\text{O}$ percentages being indicated in figure (a). The gas pressures are indicated with different marker shapes (Δ 2 kPa, \circ 10 kPa).

3.2. Density-reduced critical electric field

The density-reduced critical electric field of $\text{C}_5\text{F}_{10}\text{O}$ is about 2.1 times larger than that of SF_6 . However, due to the limited vapor pressure of $\text{C}_5\text{F}_{10}\text{O}$ only a small percentage of $\text{C}_5\text{F}_{10}\text{O}$ can be added to a carrier gas such as N_2 and CO_2 for use in electrical insulation. Therefore, synergy effects with carrier gases are, besides $(E/N)_{\text{crit}}$, an important characteristic. Mixtures of $\sim 26\%$ $\text{C}_5\text{F}_{10}\text{O}$ in N_2 and of $\sim 30\%$ $\text{C}_5\text{F}_{10}\text{O}$ in CO_2 have the same density-reduced critical electric field as pure SF_6 . However, the $\text{C}_5\text{F}_{10}\text{O}$ percentage in applications is limited by the vapor pressure of $\text{C}_5\text{F}_{10}\text{O}$. This is illustrated in figure 14, which shows the dew point of $\text{C}_5\text{F}_{10}\text{O}$ (assuming no interaction with the carrier gas) as a function of its mole fraction, for two technically relevant

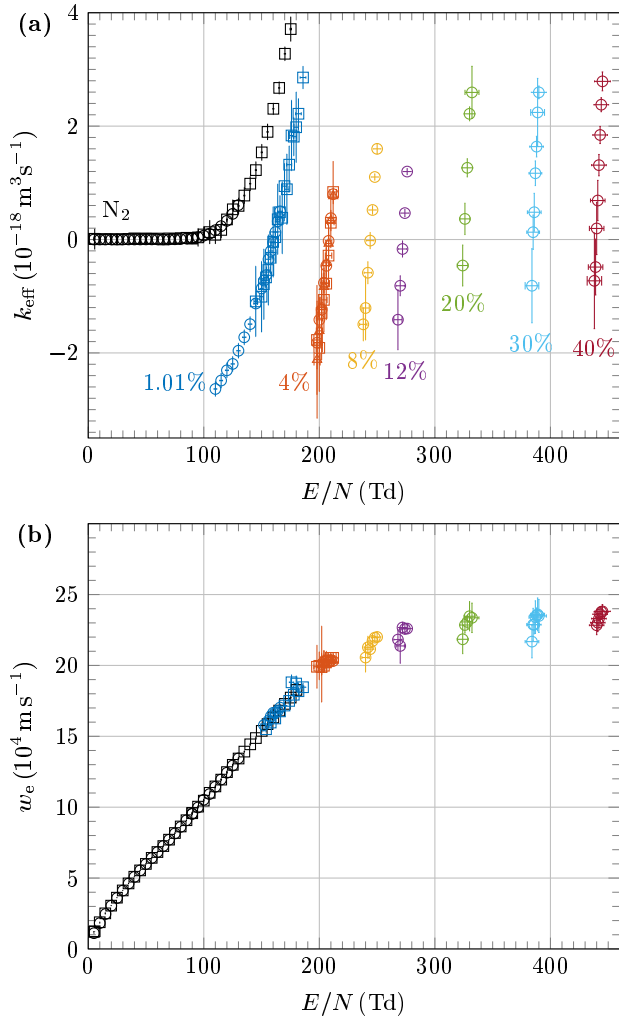


Figure 12. (a) Effective ionization rate coefficient and (b) electron drift velocity as functions of E/N in $\text{C}_5\text{F}_{10}\text{O}/\text{N}_2$ mixtures. The gas mixtures are color-coded, the $\text{C}_5\text{F}_{10}\text{O}$ percentages being indicated in figure (a). The gas pressures are indicated with different marker shapes (\square 2 kPa, \triangle 6 kPa, \circ 10 kPa).

total pressures. In order to obtain figure 14, the vapor pressure curve of $\text{C}_5\text{F}_{10}\text{O}$ was estimated by the Clausius-Clapeyron relation with a boiling point of 26.9°C and a heat of evaporation of 109 kJ kg^{-1} given by the 3M technical datasheet, and a filling temperature of 25°C was assumed. The total pressure of 0.13 MPa is typical for medium voltage applications whereas 0.6 MPa is typical for high voltage applications. For example, a current application with a minimum operating temperature of -15°C features $\text{C}_5\text{F}_{10}\text{O}$ content of 13.6% for a total pressure of 0.13 MPa [27]. It results from figure 14 that mixtures containing 2 to 27% of $\text{C}_5\text{F}_{10}\text{O}$ are of interest, depending on the targeted application. For most of these mixtures, the density-reduced critical electric field is lower than that of SF_6 . Nonetheless, it is higher

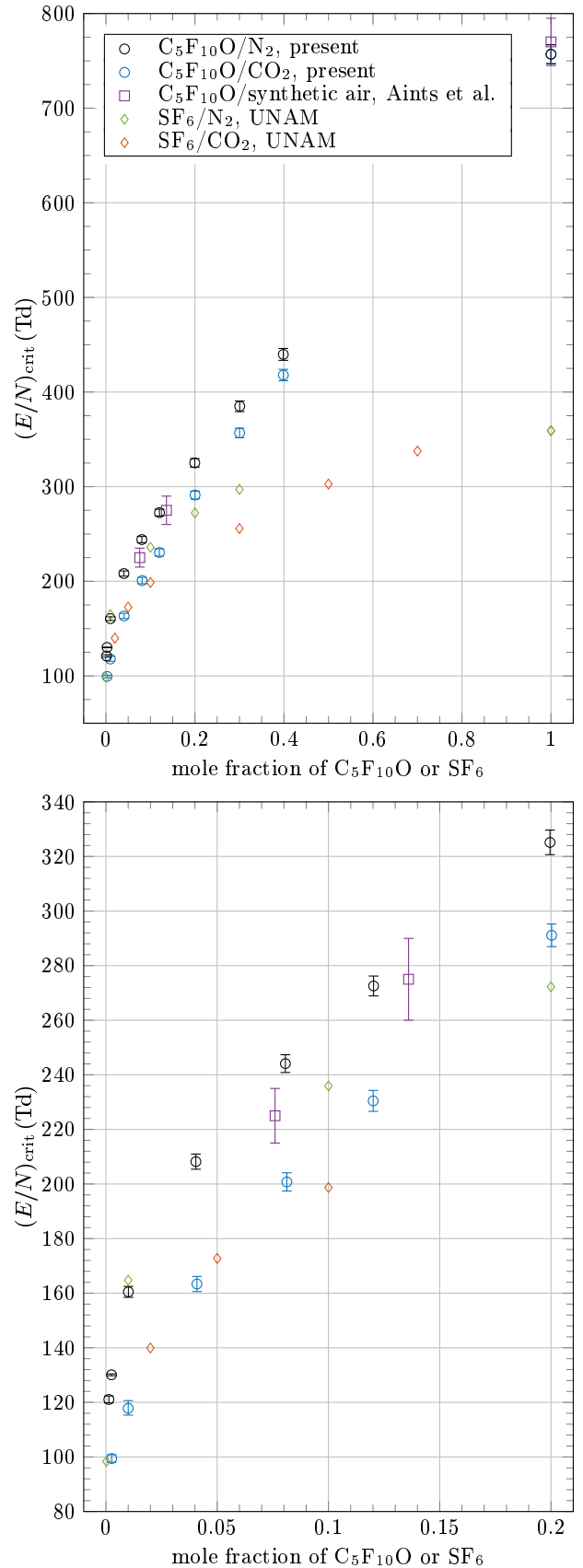


Figure 13. Density-reduced critical electric field of $\text{C}_5\text{F}_{10}\text{O}/\text{N}_2$, $\text{C}_5\text{F}_{10}\text{O}/\text{CO}_2$, SF_6/N_2 and SF_6/CO_2 mixtures.

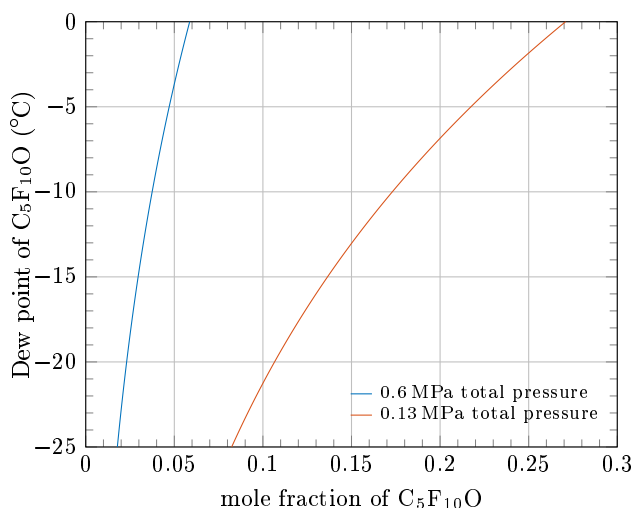


Figure 14. Dew point of $C_5F_{10}O$ as a function of its mole fraction in a gas mixture for two different total pressures of 0.13 MPa and 0.6 MPa.

than the $(E/N)_{\text{crit}}$ of synthetic air, while still having a negligible GWP.

Conclusion

We report for the first time electron rate and transport coefficients in pure $C_5F_{10}O$ and in $C_5F_{10}O/N_2$ and $C_5F_{10}O/CO_2$ mixtures, and give an estimation of the total electron attachment of $C_5F_{10}O$. We observe a synergy effect in $C_5F_{10}O/CO_2$ and $C_5F_{10}O/N_2$ mixtures leading to a relatively high density-reduced critical electric field of these mixtures even for low $C_5F_{10}O$ mole fractions. These mixtures do not offer the same density-reduced critical electric field as SF_6 , so that increasing the pressure or the insulating distance is necessary compared to SF_6 insulated devices. Nonetheless, $C_5F_{10}O$ has the advantage of having a negligible GWP and a low toxicity which is uncommon for perfluorinated molecules.

Acknowledgments

This work is financially supported by GE Grid (Switzerland) GmbH, Pfiffner Technologie AG, ABB Switzerland Ltd and Siemens AG. The sample of $C_5F_{10}O$ was provided by GE Grid Solutions, Villeurbanne, France.

References

- [1] Max-Steffen Claessens P S 2014 Dielectric insulation medium patent US8704095B2 URL <https://patents.google.com/patent/US8704095B2>
- [2] Mantilla J D, Gariboldi N, Grob S and Claessens M S 2014 Investigation of the Insulation Performance of a New Gas Mixture with Extremely Low GWP *Electrical Insulation*

Conference, Philadelphia, Pennsylvania, USA pp 469–473 ISBN 9781479927890

- [3] 3MTM NovocTM 5110 Insulating Gas, environmental, Health and Safety Summary, Issued: 6/17 URL <http://multimedia.3m.com/mws/media/14187320/12634-novec-insulating-gas-tech-bulletin-5110-a4-celum.pdf?fn=prodinfo.novec1230.pdf>
- [4] Myhre G, Shindell D, Bréon F M, Collins W, Fuglestedt J, Huang J, Koch D, Lamarque J F, Lee D, Mendoza B, Nakajima T, Robock A, Stephens G, Takemura T and Zhang H 2013 Anthropogenic and natural radiative forcing *Climate Change 2013: The Physical Science Basis. Contribution of Working Group I to the Fifth Assessment Report of the Intergovernmental Panel on Climate Change* ed Stocker T, Qin D, Plattner G K, Tignor M, Allen S, Boschung J, Nauels A, Xia Y, Bex V and Midgley P (Cambridge, United Kingdom and New York, NY, USA: Cambridge University Press) pp 659–740 ISBN 978-1-107-66182-0 URL www.climatechange2013.org
- [5] Taniguchi N, Wallington T J, Hurley M D, Guschin A G, Molina L T and Molina M J 2003 *The Journal of Physical Chemistry A* **107** 2674–2679 (Preprint <http://dx.doi.org/10.1021/jp0220332>) URL <http://dx.doi.org/10.1021/jp0220332>
- [6] 3MTM NovocTM 5110 Dielectric Fluid Data Sheet, issued 5/2017 URL https://www.3m.com/3M/en_US/company-us/all-3m-products/-/3M-Novoc-5110-Insulating-Gas?N=5002385+3291808553&rt=rud
- [7] Tehlar D, Diggelmann T, Müller P, Buehler R, Ranjan N and Doiron C 2015 Ketone based alternative insulation medium in a 170 kV pilot installation *Cigre Colloquium Nagoya, Japan* pp 223–230
- [8] Diggelmann T, Tehlar D and Müller P 2016 170 kV pilot installation with a ketone based insulation gas with first experience from operation in the grid *Cigre, Paris* pp 105–113 URL <https://e-cigre.org/publication/SESSION2016-set-of-papers--proceedings-2016-cigre-session>
- [9] Kristoffersen M, Endre T, Saxegaard M, Hyrenbach M, Wang P A, Harmsen D, van Rijn T and Vosse R 2017 *CIREP - Open Access Proceedings Journal* **2017**(1) 412–415(3) URL <http://digital-library.theiet.org/content/journals/10.1049/oap-cired.2017.0658>
- [10] Simka P and Ranjan N 2015 Dielectric strength of C5 perfluoroketone *Proceedings of the 18th International Symposium on High Voltage Engineering* URL <https://e-cigre.org/publication/ISH2015-338-dielectric-strength-of-c5-perfluoroketone>
- [11] Stoller P C, Doiron C B, Tehlar D, Simka P and Ranjan N 2017 *IEEE Transactions on Dielectrics and Electrical Insulation* **24** 2712–2721 ISSN 1070-9878
- [12] Aints M, Jögi I, Laan M, Paris P and Raud J 2018 *Journal of Physics D: Applied Physics* **51** 135205 URL <http://stacks.iop.org/0022-3727/51/i=13/a=135205>
- [13] ETHZ database URL www.lxcat.net/ETHZ
- [14] Dahl D A, Teich T H and Franck C M 2012 *Journal of Physics D: Applied Physics* **45** 485201 URL <http://stacks.iop.org/0022-3727/45/i=48/a=485201>
- [15] Häfliger P and Franck C M 2018 *Review of Scientific Instruments* **89** 023114 URL <https://doi.org/10.1063/1.5002762>
- [16] Chachereau A, Rabie M and Franck C M 2016 *Plasma Sources Science and Technology* **25** 045005 URL <http://stacks.iop.org/0963-0252/25/i=4/a=045005>
- [17] Hösl A, Häfliger P and Franck C M 2017 *Journal of Physics D: Applied Physics* **50** 485207 URL <http://stacks.iop.org/0022-3727/50/i=48/a=485207>
- [18] Chantry P J and Wootton R E 1981 *Journal of Applied Physics* **52** 2731 ISSN 00218979 URL

- 1
2
3 [http://scitation.aip.org/content/aip/journal/
jap/52/4/10.1063/1.329081](http://scitation.aip.org/content/aip/journal/jap/52/4/10.1063/1.329081)
- 4 [19] Rabie M, Haefliger P, Chachereau A and Franck C M 2015
5 *Journal of Physics D: Applied Physics* **48** 075201 URL
6 <http://stacks.iop.org/0022-3727/48/i=7/a=075201>
- 7 [20] Hagelaar G and Pitchford L 2005 *Plasma Sources Science*
8 *and Technology* **14** 722–733 ISSN 0963-0252 URL [http:
9 //dx.doi.org/10.1088/0963-0252/14/4/011](http://dx.doi.org/10.1088/0963-0252/14/4/011)
- 10 [21] Biagi database, data extracted from the fortran program
11 MAGBOLTZ of S.F. Biagi, versions 8.9 and after, data
12 retrieved on April 19, 2017 URL www.lxcat.net/Biagi
- 13 [22] Phelps database data retrieved on June 27, 2014 URL
14 www.lxcat.net/Phelps
- 15 [23] Braun M, Marienfeld S, Ruf M W and Hotop H 2009
16 *Journal of Physics B: Atomic, Molecular and Optical*
17 *Physics* **42** 125202 URL [http://stacks.iop.org/0953-
18 4075/42/i=12/a=125202](http://stacks.iop.org/0953-4075/42/i=12/a=125202)
- 19 [24] Christophorou L G and Olthoff J K 2000 *Journal of*
20 *Physical and Chemical Reference Data* **29** 267–330 URL
21 <http://dx.doi.org/10.1063/1.1288407>
- 22 [25] UNAM database data retrieved on January 27, 2017 URL
23 www.lxcat.net/UNAM
- 24 [26] Illenberger E and Meinke M C 2014 *International Journal*
25 *of Mass Spectrometry* **365-366** 80–85
- 26 [27] Hyrenbach M, Paul T A and Owens J 2017 *CIREDD -*
27 *Open Access Proceedings Journal* **2017**(1) 132–135(3)
28 URL [http://digital-library.theiet.org/content/
29 journals/10.1049/oap-cired.2017.0230](http://digital-library.theiet.org/content/journals/10.1049/oap-cired.2017.0230)
- 30
31
32
33
34
35
36
37
38
39
40
41
42
43
44
45
46
47
48
49
50
51
52
53
54
55
56
57
58
59
60